Materials Advances

ROYAL SOCIETY OF CHEMISTRY

PAPER

View Article Online
View Journal | View Issue

Cite this: *Mater. Adv.*, 2025, 6, 4402

Unveiling the nano-particle enabled synergistic mitigation of the Bcl2/Cyt *c*/CYP1A1 signaling axis as a protective therapeutic route in mitochondrial dysfunction associated diabetes†

Sudatta Dey,[ab] Rishita Dey,[ac] Priyanka Sow,[a] Banani Bhattacharjee,[a] Arnob Chakrovorty,[a] Sujan Sk,[d] Manindranath Bera,[d] Sisir Nandi,[c] Pradeepta Guptaroy[b] and Asmita Samadder*[a]

The present study aims to assess the potential benefits of bioactive chlorophyllin (CHL) and its nano-formulation against alloxan (ALX)-induced mitochondrial dysfunction, genotoxicity, and hyperglycemia. Nano-chlorophyllin (NCHL) encapsulated in poly-lactide-*co*-glycolide (PLGA) was synthesized successfully and characterized by atomic force microscopy (AFM), field emission scanning electron microscopy (FESEM), and dynamic light scattering (DLS) techniques. The strong interactions between both CHL and its nano-form (NCHL) with calf thymus DNA (CT-DNA) were further investigated by circular dichroism (CD) spectroscopy, isothermal titration calorimetry (ITC) and electronic absorption studies, demonstrating protective roles of the drug against chromosomal aberrations and micronucleus formation linked to DNA damage. The findings showed that NCHL selectively activates several proteins such as Bcl2, Cyt *c* and CYP1A1 while modulating reactive oxygen species (ROS) levels and enhancing anti-oxidative enzyme activities, including superoxide dismutase (SOD), catalase (CAT) and lipid peroxidase (LPO). This response provides a protective effect against ALX-induced oxidative stress, mitochondrial dysfunction, and hyperglycemia. Notably, NCHL also played a significant role in modulating ATP levels and the depolarization of mitochondrial membrane potential (MMP), confirming the direct influence of CHL in mitigating ALX-induced mitochondrial dysfunction and restricting the onset of hyperglycemia. Thus, our overall findings suggest that NCHL could serve as a promising drug candidate for the therapeutic management of mitochondrial dysfunction and diabetes-related complications associated with food additive exposure.

Received 7th December 2024,
Accepted 18th May 2025

DOI: 10.1039/d4ma01203h

rsc.li/materials-advances

Introduction

Diabetes, a chronic metabolic disorder affecting millions of people globally, is characterized by hyperglycemia due to insufficient insulin production or ineffective insulin response. It is classified into two main types: Type 1 diabetes mellitus (T1DM), an autoimmune condition resulting from pancreatic β cell dysfunction,[1] and Type 2 diabetes mellitus (T2DM), often linked to metabolic disorders like obesity and hypertension, leading to insulin resistance and elevated blood sugar levels.[2]

Recent dietary changes, such as increased consumption of processed food and decreased physical activity, have contributed to the rising prevalence of diabetes, especially in developing countries like India.[3] The International Diabetes Federation reported that approximately 537 million people aged between 20 and 79 years were affected by diabetes in 2021, highlighting a significant global health crisis.[4] Moreover, diabetes causes severe complications, including retinopathy, nephropathy and neuropathy, which severely impact the quality of life.[5] This "silent killer" poses a growing burden on families and communities, emphasizing the urgent need for awareness and management strategies.[6]

Urbanization has also led to increased use of food additives, raising concerns about endocrine disruption.[7] Toxicity resulting from these additives can result in oxidative stress and genotoxicity.[8] For example, aspartame may disrupt insulin receptor

[a] *Cytogenetics and Molecular Biology Laboratory, Department of Zoology, University of Kalyani, Kalyani, Nadia, West Bengal, 741235, India. E-mail: asmita.samadder@gmail.com, asmitazoo19@klyuniv.ac.in; Fax: +91 33-25828282; Tel: +91 9874548900 ext. 314/315*
[b] *Dum Dum Motijheel College, 1, Dum Dum Rd, Motijheel Avenue, Kolkata, 700074, India*
[c] *Department of Pharmaceutical Chemistry, Global Institute of Pharmaceutical Education and Research (GIPER) (Affiliated to Veer Madho Singh Bhandari Uttarakhand Technical University), Kashipur, 244713, India*
[d] *Department of Chemistry, University of Kalyani, Kalyani, Nadia, West Bengal, 741235, India*

† Electronic supplementary information (ESI) available. See DOI: https://doi.org/10.1039/d4ma01203h

function, contributing to T2DM through elevated TNFα levels and obesity.[9] Similarly, monosodium glutamate (MSG) can damage leptin receptors, increasing appetite and obesity,[10,11] while alloxan (ALX) directly destroys pancreatic β cells, hindering insulin production and raising blood sugar levels.[12,13] Current pharmacological interventions for diabetes, though effective, often have adverse side effects,[14,15] creating a demand for safer, non-toxic alternatives. Plants and their phytochemicals have been historically used because of their health benefits and low toxicity, and hence, these are increasingly explored as viable alternatives to conventional drugs.[16]

Chlorophyllin, being a non-toxic and water-soluble derivative of chlorophyll, is produced through saponification. It replaces magnesium with copper, enhancing stability for use in lower pH environments. Chlorophyllin's structure includes a hydrophilic porphyrin head and a centrally bound copper ion, making it promising for managing wound healing, oxidative stress, and blood sugar reduction.[17] It is pertinent to mention that magnesium and copper bound synthetic compounds can exhibit sugar metabolism activity, which also remains less explored.[18,19] Although effective, the low absorption and bio-availability of CHL urged for the development of drug molecules with enhanced delivery, targeted actions, high absorption and reduced cost. These combined factors of CHL have prompted the use of nanotechnology in designing advanced nano-drugs using biopolymers to enhance drug delivery, target specific actions and reduce costs. Recent research has focused on encapsulated drugs in polymer-based nanocarriers, particularly poly-lactide-*co*-glycolide (PLGA), a biodegradable and FDA-approved polymer that improves drug efficacy without altering core functionality.[20] PLGA nano-particles (0–100 nm) enhance pharmacokinetic properties and address issues such as short half-life and non-specific distribution.[21] Moreover, polymeric nanocapsules improve drug entrapment and protect against environmental factors, allowing the effective release of the active drug without degradation.[22]

This research investigates the efficacy of CHL and its nano-formulations in addressing complications related to hyperglycemia. ALX, a food additive known to induce diabetes by damaging pancreatic β cells and inhibiting glucose uptake,[23] was used to induce diabetes in both an *in vivo* (mice) and an *in vitro* (L6 rat skeletal muscle cell line) model.[24] The novel chlorophyllin (NCHL) formulation aimed to enhance drug penetration, bioavailability, and sustainability, demonstrating superior efficacy at a reduced dose compared to non-nano-forms. Its potential to delay the onset of hyperglycemia was evaluated through multi-parametric experimental approaches, assessing NCHL's ability to control genotoxicity and maintain glucose homeostasis by preserving mitochondrial function.

Materials and methods

Chemicals and reagents

All analytical grade reagents and solvents used in this research were sourced from Sigma-Aldrich and other reputable suppliers. Their usage in the tests is detailed in the text.

Preparation of PLGA encapsulated nano-chlorophyllin (NCHL)

NCHL was prepared by encapsulating CHL inside the FDA-approved biopolymer PLGA using a modified version of the solvent displacement method described by Fessi *et al.*[25,26] Briefly, 50 mg of PLGA and 20 mg of CHL were dissolved in 2 mL of acetone to create the organic phase. Separately, 1% (w/v) of poloxamer F68 (Pluronic F68) was dissolved in 20 mL of Milli-Q water under continuous magnetic stirring. The organic solution was then added dropwise to the aqueous phase at 0.5 mL min^{-1} while stirring, and the mixture was left to stir until complete evaporation of the organic solvent at room temperature.[25,27] Poloxamer F68 acted as a surfactant, aiding formation and stabilization of nano-particles by affecting their size, shape, and dispersion. After solvent evaporation, nano-particles were collected and centrifuged at 14 000 rpm for 30 min at 4 °C to remove excess stabilizer. The resulting pellets were washed with Milli-Q water three times, re-suspended, and sonicated (Labman, 35 Hz, 25 °C). The final nano-particle suspension was stored at 4 °C for future use. Blank PLGA nano-particles (without any phyto-compound core substances) were also prepared by following the same standard protocol as stated above and one arm PLGA control experiment was conducted and compared with untreated control. Since no significant changes were observed, this group was not included in further experiments.

Drug entrapment efficiency within NCHL

The encapsulation efficiency (EE%) of CHL was determined using a standard method involving quantification of unencapsulated (free) CHL in the NCHL filtrate using a UV-Vis spectrophotometer (Shimadzu UV-1800) at 450 nm.[17] The NCHL suspension was centrifuged at 11 000 rpm for 30 min at 4 °C (Remi, Mumbai, India), washed twice with Milli-Q water, and the supernatant was collected. A 100 kDa cut-off membrane filter (NANOSEP) was used to separate free CHL from the PLGA-encapsulated nano-particles present in the supernatant, following the method of Samadder *et al.*[28]

$$\text{Encapsulation efficiency (\%)} = \frac{\left([\text{Drug}]_{\text{tot}} - [\text{Drug}]_{\text{free}}\right)}{[\text{Drug}]_{\text{tot}}} \times 100$$

Characterization of NCHL through AFM (atomic force microscopy) imaging

Shape, surface and the uniformity in the spatial occurrence of the synthesized NCHL were determined from the images that were recorded through the amplitude and tapping modes of AFM (atomic force microscopy) and the free software WSxM 5.0 Develop 7.0 was utilised for data collection and image processing to create 2D and 3D plots of the synthesised nano-particle.[29]

Analysis of NCHL particles by field emission scanning electron microscopy (FESEM) with energy dispersive X-ray spectroscopy (EDX)

A newly synthesized NCHL sample in dried form was taken on a carbon conductive tape and was placed over a metallic grid. The images recorded under FESEM (GeminiSEM-450, Zeiss)

instrument confirmed the morphology and particle size. The elemental composition of the nano-particle was determined using EDX spectral analysis corresponding to the elemental energy levels.

Characterization of NCHL using a dynamic light scattering (DLS) spectroscopic study and zeta potential measurement

The DLS spectroscopic study confirmed the size distribution of the nano-particles and the zeta potential was determined using a Nano-ZS instrument (Malvern, UK) that measures the nano-particles ranging within the nano-range following the standard protocol.[28,30]

Circular dichroism (CD) spectroscopy

For this experiment, a standard DNA concentration of 1 mM was used. At 37 °C, the drug interacted with native calf thymus DNA to generate CD spectra, which were then compared to the CD spectrum of the DNA alone. Differential changes in CT-DNA (Sigma-Aldrich) structure were measured within a 200–400 nm wavelength by gradual addition of CHL and NCHL suspension following the standard protocol.[31]

CT-DNA–NCHL interaction by isothermal titration calorimetry (ITC)

This study was performed using an Isothermal Titration Calorimeter (ITC) (TA instruments, Model No. V20001) to understand the thermodynamic status of the reaction involving the drug NCHL and Calf-thymus DNA (CT-DNA). Both the CT-DNA and NCHL were dissolved in nuclease free Milli-Q water at a concentration of 0.05 mM and 0.30 mM, respectively, and the calorimetric titration was carried out at 25 °C. Prior to loading, both the drug and the DNA underwent a complete 20 min degassing to remove air bubbles from the samples and avoid the unnecessary noises in the data plot. NCHL stock solution of 0.3 mM was loaded in the syringe and was injected into 0.05 mM CT-DNA stock solution loaded in the sample cell. The titration method involved 20 injections of NCHL each of 6 μL at 400 s interval into the sample cell containing CT-DNA. The heat generated due to the dilution of NCHL in the Milli-Q water alone was subtracted from the titration data for CT-DNA–NCHL before analysis.[32] The data were analyzed using Nano Analyze v2.4.1 software using an independent site model. Analysis of the data was performed by determining the binding stoichiometry (n) and other thermodynamic parameters like enthalpy change (ΔH) and entropy change (ΔS) of CT-DNA–NCHL binding[32] using the formula: $\Delta G = RT\ln K = \Delta H - T\Delta S$.

Electronic absorption studies

One of the most effective methods for examining the binding relationship between metal complexes and nucleic acids is UV-Vis absorption spectroscopy.[33] CT-DNA may interact with molecules that have donor atoms of nitrogen, oxygen, and sulfur as well as aromatic groups.[34] The binding analysis of CHL and NCHL with CT-DNA was performed using electronic absorption spectroscopy at room temperature. The absorption titration experiments of CHL and NCHL with CT DNA were performed by measuring its effects on UV-vis spectroscopy. The experiment was accomplished by taking a fixed concentration of either CHL/NCHL (1×10^{-4} M) separately with increasing concentrations of CT-DNA (0–5.305×10^{-5} M for CHL and 0–4.368×10^{-5} M for NCHL). All solutions were prepared in 30 mM aqueous Tris–HCl buffer (pH ~ 7.5). The concentration of CT-DNA solution was determined with a molar extinction coefficient of 13 600 M^{-1} cm^{-1} at 260 nm by absorption spectroscopy.[35] This DNA concentration corresponds to the base pairs. The purity of DNA was determined by measuring the UV absorbance at λ_{max} 260 and 280 nm and then the absorbance ratio (A_{260}/A_{280}) was calculated. It was found to be in the range of 1.89–1.99, which confirmed the DNA to be sufficiently free from protein. The absorbance of DNA itself was deducted by adding an equal amount of DNA to both sample and reference solutions.

Ethidium bromide displacement studies

One useful technique for determining the modes, strength, and quenching mechanism of DNA–complex interaction is fluorescence spectroscopy. In order to further establish the binding relationship of CHL and NCHL with CT-DNA, the fluorescence emission of the ethidium bromide-bound DNA (EB-DNA) upon the addition of CHL and NCHL was monitored. Ethidium bromide displacement assay also established the DNA binding affinity of the CHL and NCHL. Primarily, CT-DNA was incubated with ethidium bromide ([EB]/[DNA] = 0.1) at 37 °C in the dark environment for 30 min. Fluorescence titrations were carried out by adding an increasing amount of CHL and NCHL from 0–3.835×10^{-3} M to 0–3.342×10^{-3} M, respectively to the cell containing the solution of the DNA/EB mixture. Emission spectra were recorded in the range of 520–700 nm at an excitation wavelength of 510 nm. The fluorescence emission bands were observed at 593 nm and 594 nm for CHL and NCHL, respectively.

Mammalian cell line culture

L6 cell lines from the National Centre for Cell Science (NCCS, Pune, India) were seeded in flasks and incubated at 37 °C with 5% carbon dioxide. The cells were cultured in Dulbecco's modified Eagle's medium supplemented with 10% fetal bovine serum (FBS) and 1% antibiotic (Gibco), maintaining a pH of 7.4. Before experiments, the cells were allowed to reach 70–80% confluency.[28]

Dose of ALX in L6 muscle cells

A concentration of 1 mM ALX was selected for a 2 h incubation period to examine the effects of hyperglycemic conditions in L6 cells.[25,28]

In vitro dose selection of CHL and NCHL

Cells were exposed to various doses of CHL for different incubation times, followed by a standard dose of ALX. A standardized dose of 30 μM CHL for 2 h incubation was selected based on intracellular glucose uptake from culture media, with NCHL doses determined as 30 μM (higher dose)

and 15 μM (lower dose), respectively, for 2 h before ALX treatment.

Evaluation of glucose uptake in L6 cells

Glucose uptake in different experimental sets of L6 cells was estimated using the standard GOD-POD kit protocol.[36] The media glucose concentration was used to analyse hyperglycemic conditions in the experimental sets.[28]

Investigation of DNA damage by DNA fragmentation assay

The ability of NCHL to prevent ALX-induced DNA-damage in L6 cells of different experimental groups was determined by DNA isolation using phenyl-isoamyl-chloroform and 1% gel electrophoresis following the standard protocol.[37]

Analysis of DNA damage and nuclear condensation in L6 cells

L6 cells were stained with PI and DAPI to assess nuclear morphology changes *via* fluorescence intensity. The cells were treated with each stain independently and incubated for 15 min at 4 °C. Images were recorded under a Carls Zeiss LSM 800 confocal microscope at 10X magnification.[28]

Immunofluorescence detection of Cyt *c*, Bcl2 and p53 proteins in the L6 cell line

Protein expressions of Cyt *c* and Bcl2, which are mitochondrial membrane proteins, and p53, which is a DNA damage response protein responsible for activating the mitochondria-induced apoptotic pathway, were estimated in different experimental sets using anti-Cyt *c*, anti-Bcl2 and anti-p53 primary antibodies, along with FITC-labeled secondary antibodies. The images were observed under a confocal microscope (Carl Zeiss LSM 800).[28]

Model animal

Healthy male Swiss albino mice (*Mus musculus*), aged 12–14 weeks and weighing 30–34 g, were acquired from West Bengal Livestock Development Corporation Ltd in Kalyani. The mice were acclimatized for 1–2 weeks under optimal conditions (12 h light/dark cycle, 25 ± 2 °C, 55 ± 5% humidity) and were maintained on a standard diet with water *ad libitum*, following CPCSEA guidelines. Experiments were conducted with care under the Institutional Animal Ethics Committee of Kalyani University (IAEC-KU) supervision and approval (892/GO/Re/S/01/CPCSEA; Pr: 20.4.14-28.4.2019).

Diabetes induction in mice

Diabetes was induced in mice by a single intraperitoneal injection of alloxan monohydrate (ALX) (CAS No. A7413) at a dose of 100 mg kg^{-1} b.w. after 12 h starvation.[38] The mice were then allowed to drink a 5% glucose solution overnight.[39]

Dose selection of CHL and NCHL

A range-finding trial was previously conducted to determine the effective dose of CHL in mice, with groups receiving 10 mg kg^{-1} and 70 mg kg^{-1} body weight (b.w.). by oral gavage. The chlorophyllin (CHL) pre-treated mice received an intraperitoneal injection (i.p.) of ALX at a dose of 100 mg per kg b.w. thereafter. The dose of 50 mg kg^{-1} was selected based on its glucose-lowering effects and cell viability.[40] After standardization of the CHL dose, the mice groups received doses of nanochlorophyllin (NCHL): 50 mg per kg b.w. and 25 mg per kg b.w. on alternate days for 1 month followed by intra-peritoneal injection of ALX after an interval of 7 days.

Release kinetics of NCHL with time

To determine the minimum time required for CHL release from PLGA-encapsulated NCHL in mice, a time-dependent release kinetics study was conducted. Prior to the experiment, NCHL pellets were suspended in PBS and a standard calibration curve was generated by measuring the absorbance of NCHL solutions (10–300 nM) at 450 nm using a UV-Vis spectrophotometer (Shimadzu UV-1800). Mice were orally administered with a lower dose of NCHL and sacrificed at predetermined time points (0, 12, 24, 48 and 96 h). Pancreatic tissues were harvested, homogenized in ice-cold PBS, and centrifuged at 12 000 rpm for 12 min. CHL levels in the supernatants were quantified spectrophotometrically.[41] The release ratio was calculated based on absorbance values corresponding to each time point.

Experimental design

Five different groups were formed from the randomly selected experimental sets. Each set contained 3 mice:

Group I: control group
Group II: ALX administered group
Group III: pre-treatment of CHL (50 mg kg^{-1} b.w.) + ALX
Group IV: pre-treatment of NCHLI (50 mg kg^{-1} b.w.) + ALX
Group V: pre-treatment of NCHLII (25 mg kg^{-1} b.w.) + ALX

Estimation of blood glucose levels from experimental sets

Blood glucose levels in different experimental sets were checked using a Standardized GOD-POD Glucose kit (Autospan) purchased from Arkray Healthcare Pvt. Ltd, India (Code: 93DP100-74).[36]

Oral glucose tolerance test

The oral glucose tolerance test (OGTT) was conducted across experimental groups following the standard protocol,[42] with minor modifications. 24 h after confirmation of diabetes induction, mice were fasted overnight. Control and alloxan (ALX)-treated diabetic mice received either drinking water or the respective treatments (CHL or NCHL) orally, followed by an intraperitoneal glucose injection at a dose of 3 g per kg body weight. Blood samples were collected prior to treatment and at designated intervals post-glucose administration. Glucose levels were assessed spectrophotometrically by measuring absorbance at 505 nm.

Cell viability study of hepatic and pancreatic tissue

After sacrificing the mice from different experimental groups, cell viability in isolated liver and pancreatic tissues was assessed using the Trypan Blue dye-exclusion method. Blank PLGA nano-particles, prepared without CHL, were tested on

alloxan-treated mice for protective effects against cytotoxicity but showed no efficacy. Cell viability tests confirmed their lack of efficacy in the model organisms.[25] The percentage of cell viability was calculated using a standard formula:

$$\%\ \text{cell viability} = \frac{\text{Number of viable cells}}{\text{Total number of cells}} \times 100$$

Determination of histopathological changes and morphometric analyses of pancreatic islets

Histological samples were prepared by fixing, blocking, and sectioning tissues from autopsied mice. The tissues were then counter-stained with hematoxylin–eosin following standard protocols[43] and examined under a compound light microscope. Morphometric analysis of pancreatic islets was performed to assess cellular density in mice models of ALX-mediated diabetes. Morphometric analysis was conducted using ImageJ software from the images recorded at 40X magnification to quantitatively evaluate islet density in a fixed area.[44]

Determination of total cholesterol from hepatic tissues

A colorimetric assay kit supplied by Span diagnostics Ltd, Sachin, Surat, India, code – old: LG051, New: 71LS200-40 was used to estimate the cholesterol levels in the liver homogenates obtained from the control and different experimental sets of mice following the protocol of Kaplan and Lavernel (1983).[45]

Analysis of hepatotoxicity biomarker enzymes

The biomarker enzyme levels, specifically aspartate transaminase (AST) and alanine transaminase (ALT), were measured in hepatic tissue suspensions to assess hepatotoxicity and the extent of hepatic injury, following the standard protocol of Bergmeyer and Brent (1974).[46]

DNA fragmentation assay

Genomic DNA was extracted from pancreatic tissues using the phenol-chloroform method. DNA fragmentation was evaluated by 1% agarose gel electrophoresis,[37] showing differential band smearing under a UV transilluminator (GENEI).[47]

Comet assay

To ascertain the degree of DNA damage in single cells, the visual analysis using DNA staining by ethidium bromide dye was used and observed under a fluorescence microscope (Carl Zeiss Axio Vert A1-FL-LED). The calculation of the frequency of comet tailed cells was performed from the images captured. The comet assay was carried out using single-cell gel electrophoresis following the protocol.[48] As described earlier, single-cell gel electrophoresis was used to carry out the comet assay for the estimation of DNA damage.[49]

Assessment of chromosomal aberrations

Colchicine (0.03%) was administered intraperitoneally to mice at 1 mL per 100 g b.w. and kept for 1 h and 10 min before sacrifice. Bone marrow cells from different experimental groups were analyzed for chromosome spreads using standard protocols.[26,31,40] Metaphase spreads were stained with Giemsa and examined microscopically for cytogenetic abnormalities, facilitating a detailed analysis of chromosomal changes across the groups.[50]

Estimation of micronucleus formation

Following colchicine treatment, bone marrow cells were considered for the micronucleus study from different experimental sets of mice following the standard procedure.[50] Approximately about 1000 bone marrow cells were analysed from each experimental set to determine micronucleated polychromatic erythrocytes (MnPCEs) for the cytogenetical assessment.[40]

Estimation of anti-oxidative enzyme profiles

The activity of antioxidative enzymes like lipid peroxidase (LPO), catalase (CAT), and superoxide dismutase (SOD) was assessed in pancreatic tissue from both control and experimental groups. The procedure involved homogenizing the tissue in cold PBS, centrifuging for 30 min at 11 000 rpm, and storing the suspension at −80 °C. Standard protocols were followed for LPO,[51] SOD,[52] and CAT.[53]

Analysis of ROS generation from pancreatic cell suspension

To assess the redox state of cells, isolated pancreatic cells were fixed in 4% paraformaldehyde and incubated with H_2DCFDA dye for 30 min at room temperature. Reactive oxygen species (ROS) levels were measured using a spectrofluorometer (Hitachi F-7100) at 485 nm (excitation) and 535 nm (emission) following standardized protocols.[54–56]

Assessment of MMP using Rhodamine 123 dye

Isolated pancreatic cell suspensions were incubated with Rhodamine 123 (Rh 123) for 15 min at 4 °C to assess mitochondrial membrane potential (MMP, $\Delta\psi m$) across different experimental groups. MMP was measured spectrofluorometrically at 480 nm (excitation) and 535 nm (emission) following standard protocols.[28]

Determination of ATPase levels

ATPase enzyme levels were measured in pancreatic tissues from all experimental groups, including the control group. Quantitative estimation was conducted using the conventional methodology.[57]

Detection of calcium ions by the complexometric titration method

To estimate calcium ions, pancreatic tissue suspensions from control and various experimental groups were titrated using the standard protocol[28] with the disodium salt of EDTA and the indicator Eriochrome Black T (EBT).

Immunofluorescence detection of Bcl2, Cyt *c* and CYP1A1 proteins

Bcl2, Cyt *c* and CYP1A1 proteins were detected through immunofluorescence, and the pancreatic tissue sections were counter-

stained using propidium iodide (PI). Expression of the proteins was assessed with anti-Bcl2, anti-Cyt *c* and anti-CYP1A1 primary antibodies and FITC (Fluorescein-5-isothiocyanate) labeled secondary antibodies, under an epifluorescence microscope.[28]

Statistical analysis

All experiments were independently repeated three times before statistical analysis. Data were collected, and the standard error of the mean was calculated. Statistical significance was assessed using Student's *t*-test and one-way ANOVA using Graphpad software, with results indicated as follows: $***p < 0.001$, $**p < 0.01$ and $*p < 0.05$ *vs.* ALX considered significant as per Student's *t*-test.

Results and discussion

Physico-chemical characterization of PLGA-encapsulated NCHL

After formulation of the nano-particles (NPs), the synthesized materials underwent physico-chemical characterization using the standard atomic force microscopy technique, revealing the morphological and topographical characteristics of NCHL. The 2D image verified the spherical shape of NCHL (Fig. 1a), while the 3D image suggested that the formed nano-particles had a smooth surface free of any fissures or crevices (Fig. 1b). The mean diameter of the PLGA-encapsulated nano-chlorophyllin (NCHL) was found to be approximately 60 ± 0.05 nm by the height profile analysis (Fig. 1c). The uniformity in the spatial frequency of the similarly sized nano-particles from the topographic signal was confirmed by the 2D view of the Fast Fourier Transform (FFT) study obtained from AFM data (Fig. 1d). Furthermore, the FESEM image confirmed the spherical shape of NCHL particles (Fig. 1e); the EDX spectra analysis verified the elemental composition and purity of the freshly synthesised NCHL free of metallic contamination as shown by the carbon and oxygen peaks (Fig. 1f). The PLGA-encapsulated CHL (NCHL) size distribution was confirmed by DLS data, which showed that its mean diameter was between 0 and 100 nm. Furthermore, when NCHL is in the solution state, the polydispersity index (PDI) value of 0.529 indicates the formation of a homogenous suspension (Fig. 1g). Additionally, the negative zeta value of −10.1 mV indicates that NCHL particles were stable inside of cellular compartments (Fig. 1h). From the graphical plot, % encapsulation efficiency (%EE) of CHL within the polymeric PLGA capsules to form NCHL was calculated as 86.24% (Fig. 1i). Moreover, the *in vivo* release kinetics of NCHL

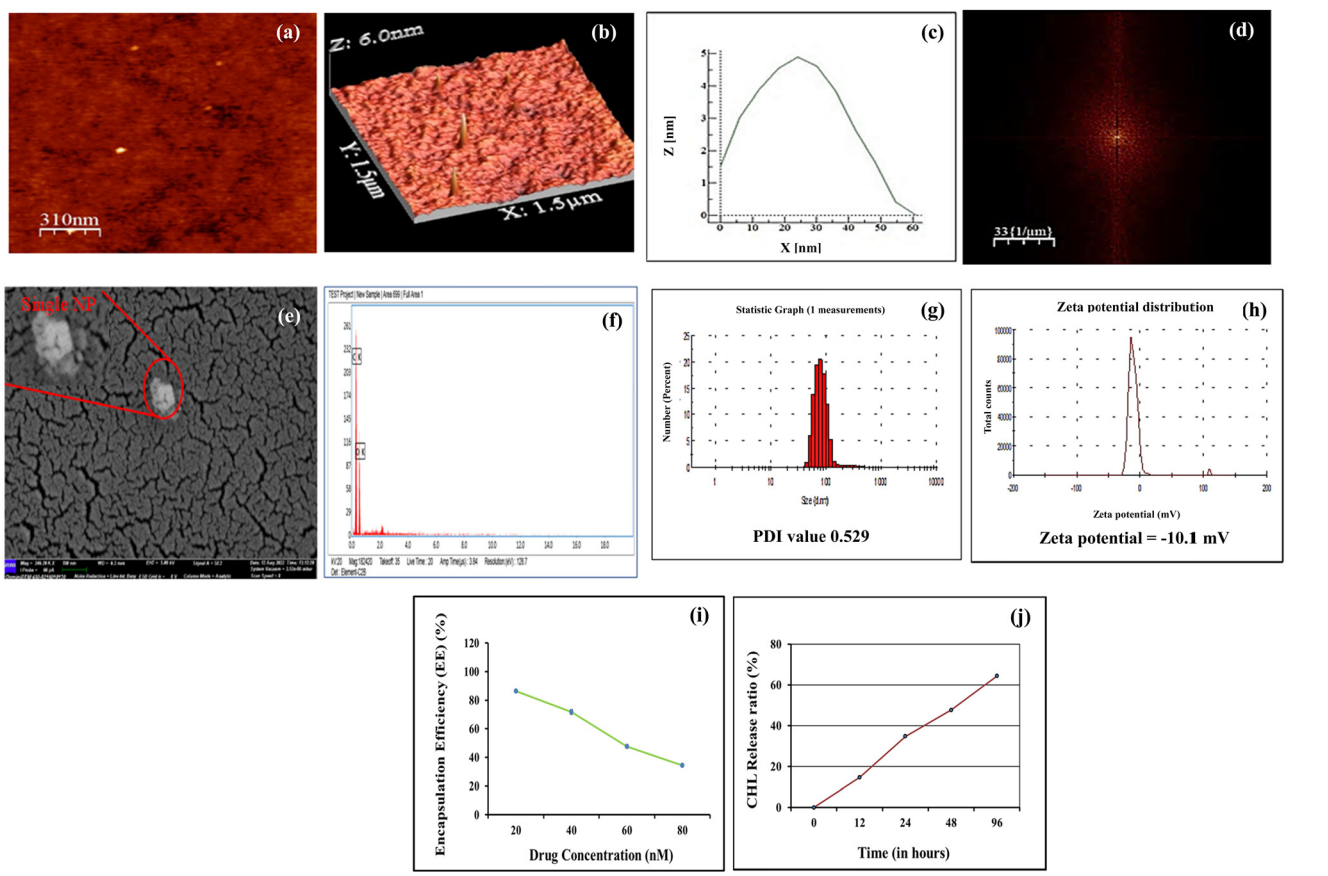

Fig. 1 (a)–(d) AFM images of NCHL: (a) 2D view of NCHL, (b) 3D view of NCHL, (c) size profile of NCHL, (d) FFT analysis, (e) FESEM image of NCHL, (f) EDX spectra of NCHL, (g) DLS spectroscopy showing the average diameter of NCHL within 0–100 nm with a PDI value of 0.529, (h) zeta potential of NCHL, (i) graphical representation of % encapsulation efficacy (%EE) of CHL in PLGA-Nps with increasing amount of drug (CHL), and (j) *in vivo* release kinetics of NCHL.

demonstrated a suspended release profile of CHL over time. By the 96th hour, approximately 64.33% of the encapsulated drug had been released from the nano-particles, indicating a prolonged and controlled release behavior (Fig. 1j). Our findings demonstrated that PLGA-encapsulated nano-particles synthesized *via* the solvent displacement method, exhibited optimal physico-chemical properties for effective drug delivery. This nano-formulation approach significantly improved CHL release kinetics, addressing challenges related to controlled drug release, and thereby enhancing its absorption, bioavailability, and tissue distribution, even at reduced doses. The nano-particles owing to its size within 1–100 nm and a negative surface charge (zeta potential) showed reduced agglomeration and improved cellular uptake through modulation of cell membrane potential, without compromising cellular integrity. Furthermore, the incorporation of F68 as a stabilizer enhanced encapsulation efficiency, particle homogeneity, and overall stability, supporting the therapeutic efficacy and prolonged shelf-life of NCHL. These results collectively highlight the potential of PLGA-based nanocarriers in improving targeted drug delivery and therapeutic outcomes against toxicant-induced pathologies.

Bio-physical interaction of DNA with CHL and NCHL

Bio-physical interaction of drug and DNA could be ascertained from the circular dichroic spectra of calf-thymus DNA analysis where base stacking and helicity changes in the B-form DNA structure are typically indicated by a positive absorbance intensity of CT-DNA in the region of 273 nm and a negative absorbance intensity at approximately 245 nm, respectively. Upon addition of CHL and NCHL separately to the CT-DNA, a discernible increase in the molar ellipticity of the DNA was noticed with a positive spectral shift at the region between 265–280 nm and a much negative spectral shift at around 245 nm, in the case of NCHL. The overall result indicated that NCHL has a strong affinity for CT-DNA (10-fold lower dose of CHL) compared to CHL alone (Fig. 2a), and this affinity was maintained without altering the DNA's B-form conformation, since no negative intensity peak was obtained at the 212 nm region. Another bio-physical study was performed that investigated both the kinetic and thermodynamic aspects of drug–DNA interaction. The isothermal titration calorimetric method comprehends the interaction and binding forces involved in the biological milieu (Fig. 2b). The thermodynamic parameters, binding constant (K_a), enthalpy change (ΔH), entropy change (ΔS), and the number of binding sites (n), inferred after baseline correction, happen to be part of the binding profile of NCHL to CT-DNA. It was found from our experiments that the values of ΔH, ΔS, and K_a were -1.587 kJ mol^{-1}, 112.5 J mol^{-1} K^{-1}, and 1.432 $\times$ 106 mol L^{-1} respectively. The Gibb's free energy change was measured using the following equation: $\Delta G = -RT\ln K = \Delta H - T\Delta S$, where T denotes absolute temperature in the Kelvin scale, which equals 298.15 K, R denotes the gas constant, which equals 8.314 J K^{-1} mol^{-1}. The value of ΔG was determined to be -35.137 kJ mol^{-1} using the equation. As shown in Fig. 2b, the formation of the CT-DNA–NCHL complex was exothermic, evidenced by the negative enthalpy change (ΔH). The negative Gibbs free energy (ΔG) further confirmed a strong, spontaneous interaction between NCHL and CT-DNA, indicating that the binding process was enthalpy-driven. Furthermore, to evaluate the binding interactions between CHL and NCHL with CT-DNA, electronic spectroscopic studies were performed where the spectral changes occurring in the range of 210–500 nm have been examined. In these experiments, a fixed concentration of CHL and NCHL was titrated by increasing the concentrations of CT-DNA at pH $\sim$7.5 as displayed in Fig. 2c and d, respectively. As shown in Fig. 2c and d, upon the addition of CT-DNA, the CHL shows a significant red shift for CT-DNA with a corresponding increase of the absorption band at 238 nm. Also, the NCHL exhibits a significant red shift for CT-DNA, with a corresponding increase of the absorption band at 238 nm. The UV-vis spectra clearly show significant hyperchromism of the higher energy band at 238 nm for both CHL and NCHL due to the interaction between the CHL moiety and DNA bases. Such binding reduces the base stacking interaction and causes an increase in their absorption intensity. On the other hand, the lower energy UV band at 404 nm for both CHL and NCHL exhibits insignificant hypochromism with a slight red shift of the absorption maximum upon DNA binding. Usually, the extent of both hyperchromism and hypochromism is associated with the strength of DNA binding. As observed from the UV-vis titration spectra, the percentage of hyperchromism was $\sim$49% for CHL and $\sim$56% for NCHL, implying their decrease in DNA binding affinities in the order, NCHL $>$ CHL. To evaluate the relative binding strength of the CHL and NCHL with CT-DNA, the binding constant (K_b) values were calculated by using the following equation: $[DNA]/(\varepsilon_a - \varepsilon_f) = [DNA]/(\varepsilon_b - \varepsilon_f) + 1/K_b\ (\varepsilon_b - \varepsilon_f)$ (where [DNA] = concentration of CT-DNA, ε_a = ratio of the absorbance/[CHL or NCHL], ε_f = extinction coefficient of free CHL or free NCHL, and ε_b = extinction coefficient of CHL or NCHL when fully bound to DNA). Usually, a plot of $[DNA]/(\varepsilon_a - \varepsilon_f)$ *vs.* [DNA] gives a slope and an intercept equal to $1/(\varepsilon_b - \varepsilon_f)$ and $1/K_b\ (\varepsilon_b - \varepsilon_f)$, respectively, and the binding constant K_b is obtained as the ratio of the slope to the intercept. The calculated binding constant (K_b) values in the interaction of CHL and NCHL with CT-DNA are found to be $(4.191 \pm 0.264) \times 10^3$ M^{-1} and $(5.769 \pm 0.392) \times 10^3$ M^{-1}, respectively (Fig. 2c and d (inset)). Electronic absorption spectral analysis suggests that both CHL and NCHL are capable of binding to CT-DNA, likely through partial intercalation or groove-binding modes, with comparable binding affinities. However, further experimental validation was required to conclusively determine the precise mode of interaction. Additionally, ethidium bromide displacement studies revealed a marked increase in fluorescence intensity in the presence of DNA, consistent with EB's strong intercalation between DNA base pairs. If the metal complexes or small drugs displace EB from the DNA-bound EB, the fluorescence intensity decreases because the free EB molecules are much less fluorescent than the DNA bound EB molecules because the surrounding water molecules quench the fluorescence of free EB. A reduction in the intensity of the emission spectra was observed when an aqueous solution of CHL and

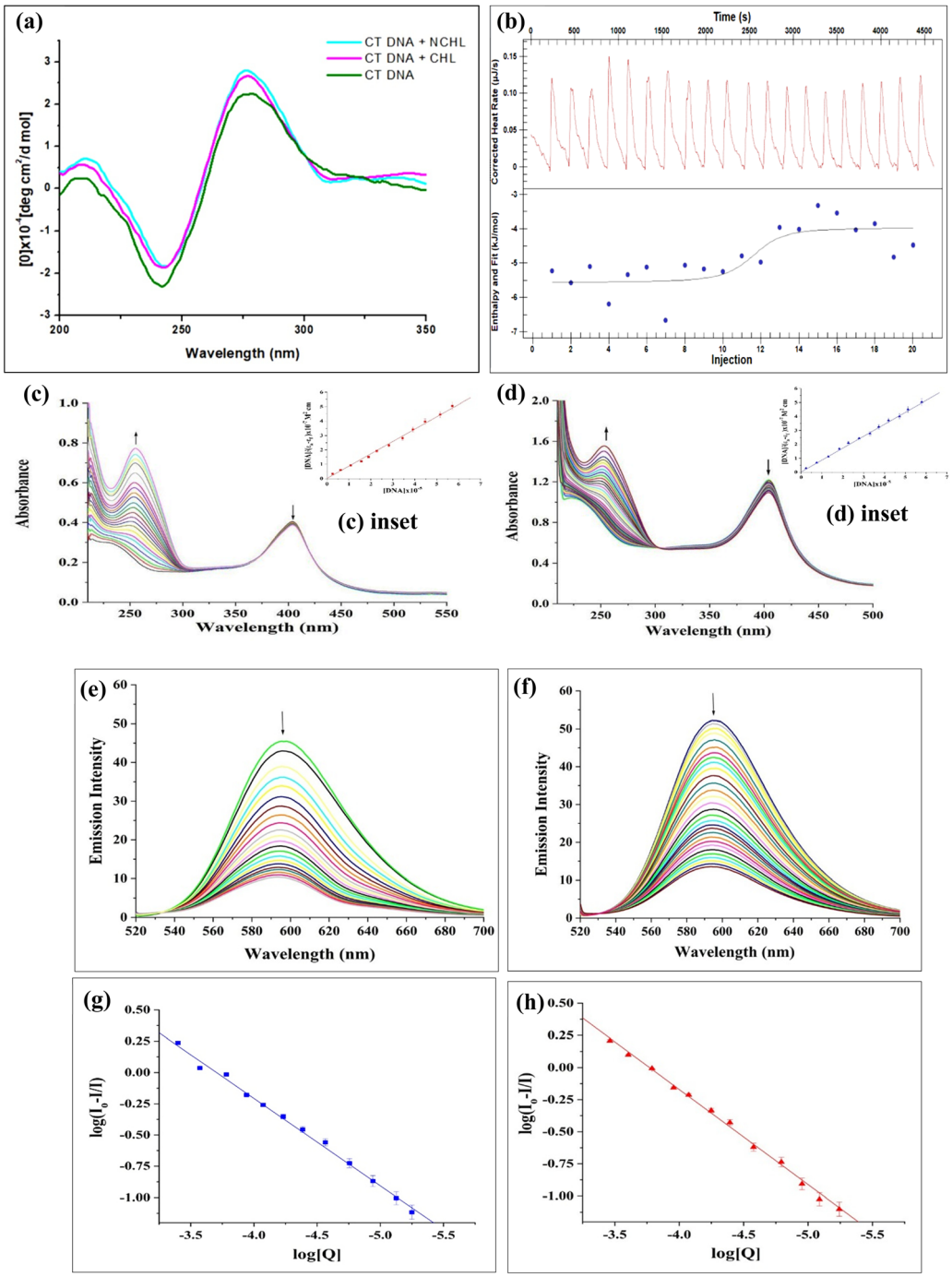

Fig. 2 DNA binding studies: (a) CD spectral analysis of CT-DNA binding with CHL and NCHL, (b) ITC profile of CT-DNA and NCHL. CT-DNA (0.05 mM) titration done by the subsequent addition of NCHL (0.3 mM) solution. The upper panel shows the corrected calorimetric profile of the injection of solution into CT-DNA solution and the lower panel shows the ITC enthalpogram along with the best fit line as monitored at 298.15 K in Milli-Q water, (c) and (d) UV-vis absorption spectral changes of (c) CHL and (d) NCHL (1×10^{-4} M) in 30 mM Tris–HCl buffer at pH ~ 7.5 in the presence of increasing concentrations of CT-DNA (0–5.305×10^{-5} M for CHL and 0–4.368×10^{-5} M for NCHL). (inset) The binding profile of [DNA]/($\varepsilon_a - \varepsilon_f$) *vs.* [DNA] for (c) CHL and (d) NCHL, (e) fluorescence emission spectral changes of ethidium bromide (EB) bound to CT-DNA in the presence of increasing concentrations of CHL in 30 mM Tris–HCl buffer at pH 7.5 (λ_{exi} = 510 nm; λ_{emi} = 593 nm). Arrow signifies the changes that occurred in the emission intensity upon the addition of the increasing concentrations of CHL, (f) fluorescence emission spectral changes of ethidium bromide (EB) bound to CT-DNA in the presence of increasing concentrations of NCHL in 30 mM Tris–HCl buffer at pH 7.5 (λ_{exi} = 510 nm; λ_{emi} = 594 nm). Arrow signifies the changes occurred in the emission intensity upon the addition of the increasing concentrations of NCHL, (g) Scatchard plot of log[($I_0 - I$)/I] *vs.* log[Q] for CHL, and (h) Scatchard plot of log[($I_0 - I$)/I] *vs.* log[Q] for NCHL.

NCHL was added. This is shown in Fig. 2e and f. Upon the addition of equal volumes of aliquots of CHL and NCHL with a fixed concentration of ethidium bromide-bound DNA (EB-DNA), a significant quenching of the emission intensity at 596 nm has been observed. This hypochromic effect in the fluorescence titration implies that EB may be partially replaced from the EB/DNA system, and the binding may involve some groove binding mode or partial intercalative mode. When small molecules bind separately to a set of identical sites on a macromolecule, some will remain in the bound state and some will remain in the unbound state. So, the equilibrium between unbound and bound molecules can be described by the Scatchard equation: $\log[(I_0 - I)/I] = \log[K] + n\log[Q]$, in which K and n are the binding constant and the number of binding sites, respectively, and I_0 and I are the fluorescence intensities in the absence and presence of the quencher, respectively. Hence, the plots of $\log[(I_0 - I)/I]$ *vs.* $\log[Q]$ (Fig. 2g and h) can be utilized to have the binding constant values, which are evaluated to be $(3.886 \pm 0.14) \times 10^2\ M^{-1}$ and $(6.193 \pm 0.08) \times 10^2\ M^{-1}$ for CHL and NCHL, respectively. Again, the comparison of binding constant values suggests that DNA binding affinities follow the order: NCHL > CHL. Preliminary insights from circular dichroism (CD) spectroscopy revealed conformational changes in DNA upon interaction with NCHL, indicating strong and favorable CHL binding even at low concentrations. This was further supported by the negative Gibbs free energy values obtained from isothermal titration calorimetry (ITC), confirming the spontaneity of the interaction. Additionally, electronic absorption spectroscopy demonstrated hyperchromism accompanied by notable bathochromic shifts, suggesting that NCHL interacts directly with DNA bases in an enthalpy-driven, spontaneous manner, consistent with the concentration-dependent binding behavior observed in the ITC analysis and EtBr displacement studies.

CHL and NCHL in attenuating genotoxicity

The favourable outcomes from biophysical interaction studies with both CHL and NCHL prompted further evaluation of their protective effects against oxidative stress induced genotoxicity due to ALX treatment in both *in vivo* and *in vitro* models. To assess the drug's impact on DNA structural integrity, a series of biological and parametric analyses were conducted. DNA damage by fragmentation is one of the determining markers of genotoxicity caused by any kind of toxicant. In this investigation, the DNA damage is measured quantitatively using DNA fragmentation assay where the intensity of DNA fragmentation of genomic DNA isolated from pancreatic tissues determines the magnitude or the extent of DNA damage. Upon comparing the gels of DNA smears obtained from control and different experimental groups of mice, the results indicated a substantial lowering of DNA smearing in the case of the NCHLI + ALX group compared to ALX-induced DNA damage in pancreatic tissue. Again, from the figure, it was very evident that as compared to the CHL dose, the NCHLI dose showed better protection against ALX-induced DNA smearing and damage even at a reduced dosage amount in pancreatic tissue (Fig. 3a). A similar study was performed in L6 cells across control and experimental groups. Results showed a similar result with the nano-drug pre-treatment providing superior protection against ALX-induced DNA damage compared to CHL, even at lower doses. In ALX-treated groups, DNA smearing was markedly enlarged compared to controls (Fig. 3b). The effect of genotoxicity was further investigated in single cells isolated from the pancreatic tissue. The extent of DNA damage was measured by comparing the frequency of comets encountered in cells isolated from the pancreatic tissues obtained from control and different experimental groups of mice. An increase in the lengths of comets in the ALX treated groups signified greater DNA damage; but in the hyperglycemic mice pre-treated with CHL and NCHL, the length and frequency of comet tails significantly decreased, although NCHLI doses gave a better protection against ALX-induced DNA damage than other drug pre-treated groups (Fig. 3c). For determining a large-scale DNA damage, the morphology of each chromosome was scored in order to ascertain any form of aberration occurring due to presence of the toxicant-ALX. When compared to the control group, the administration of ALX was found to cause a variety of chromosomal aberrations (CAs), including ring chromosome, chromatid breakage, terminal deletion, stretching, *etc.* (marked with red colour arrowheads). However, compared to the CHL pre-treatment + ALX groups, the frequency of CA was found to be significantly lower in the NCHL pre-treated + ALX groups, indicating a better protective role of NCHL than CHL against ALX-induced CA and genotoxicity (Fig. 3d and e). Additionally, scoring of the micro-nucleated polychromatic erythrocytes (MnPCEs) in control and various experimental mice groups exhibited a higher frequency of MnPCEs in the diabetic mice group. On the other hand, the mice in the CHL and NCHL pre-treated groups had lower MnPCE frequencies than the ALX-treated group, suggesting increased potential of NCHL for limiting ALX induced genotoxicity and MnPCE formation (Fig. 3f). Furthermore, genotoxicity was analysed in L6 cells of different experimental groups by detecting DNA damage and nuclear condensation using DAPI and PI dye respectively. From our investigation, it was found that pre-treatment with CHL and NCHL prior to ALX exposure reduced DNA damage and alleviated nuclear condensation in L6 cells compared to the ALX-only group. Propidium iodide (PI) intensities indicated that NCHL offered better protection against ALX-induced DNA damage and nuclear condensation than CHL (Fig. 3g). Additionally, DAPI staining confirmed that NCHL pre-treatment resulted in lower genotoxicity (Fig. 3h), which is pictorially represented by intensity graphs of the respective fluorescence observations (Fig. 3i and j). Collective evidence from CD spectroscopy indicates a strong binding of CHL to DNA, protecting against ALX-induced oxidative DNA damage, as evidenced by reduced comet tail formation in pancreatic cells and decreased chromosomal aberrations, MnPCEs in mice, and nuclear condensation in L6 cells. These effects likely result from CHL–DNA binding, which prevents ALX interaction with DNA. The occurrence of chromosomal aberrations and micronuclei under ALX-induced diabetic stress serves as

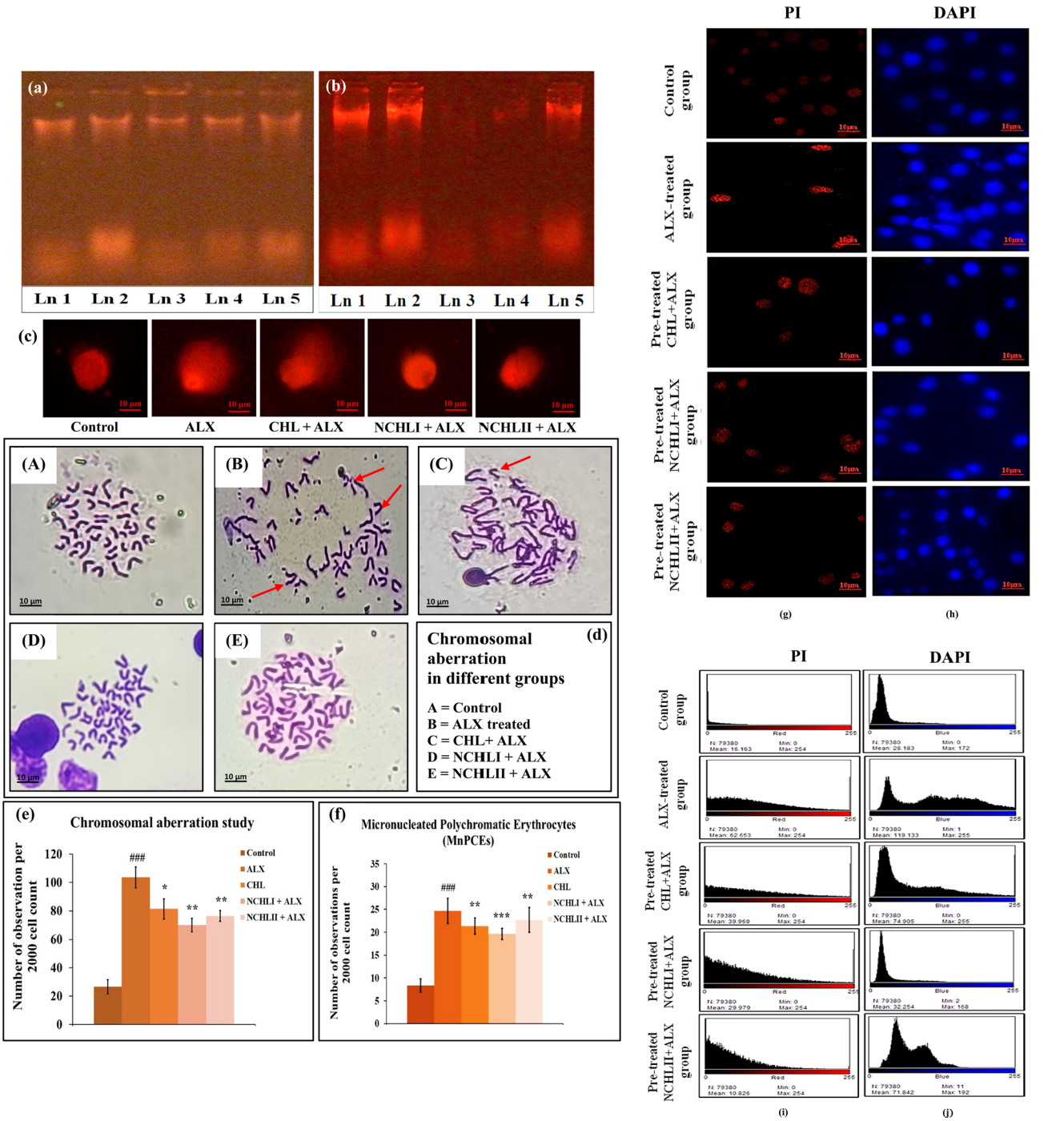

Fig. 3 DNA damage assessment: (a) assessment of DNA damage by fragmentation assay in control and different experimental pancreatic tissues. (b) Assessment of DNA damage by fragmentation assay in control and different experimental groups of L6 cells. Ln 1: control, Ln 2: ALX, Ln 3: CHL + ALX, Ln 4: NCHLI + ALX, Ln 5: NCHLII + ALX, (c) pictorial representation of DNA damage by Comet assay, (d) representative images of normal and aberrant metaphase somatic chromosomal plates in experimental groups of mice. (A) Control; (B) ALX-treated group; (C) CHL + ALX treated group; (D) NCHLI + ALX treated group; (E) NCHLII + ALX treated group. The marked area with red-coloured arrowheads in image B and C shows varieties of structural aberrations in chromosomes, (e) graphical representation showing the occurrence of chromosomal aberrations (CAs). $^{###}p < 0.001$ *vs.* control, $^{**}p < 0.01$ *vs.* ALX, $^{*}p < 0.05$ *vs.* ALX; were considered significant for Student's *t*-test, (f) graphical representation of frequency of micro-nucleated polychromatic erythrocytes (MnPCEs) in bone marrow cells of different groups. $^{###}p < 0.001$ *vs.* control, $^{**}p < 0.01$ *vs.* ALX, $^{***}p < 0.001$ *vs.* ALX were considered significant for Student's *t*-test, (g) analysis of nuclear condensation in L6 cells by PI dye, (h) analysis of DNA damage in L6 cells by DAPI fluorescence, (i) intensity plots of L6 cells of different experimental groups stained with PI stain, and (j) intensity plots of L6 cells of different experimental groups stained with DAPI stain.

a biomarker of impaired DNA repair, often linked to dysfunction of key regulatory proteins such as p53. This is supported by observed alterations in DNA structure and associated stabilizing proteins following CHL pre-treatment, suggesting activation of DNA repair pathways involving p53 protein, reinforcing its role in genomic stability. Thus, NCHL's ability to inhibit oxidative genotoxicity suggests its potential to prevent apoptosis in both pancreatic cells and L6 cells (Fig. S1e and f, ESI†), supporting the therapeutic role of CHL nanoformulation.

CHL and NCHL role in inhibiting mitochondrial dysfunction

Rhodamine 123 (Rh123) is a cationic, cell-permeable fluorescent dye that selectively accumulates in polarized mitochondria due to the negative membrane potential. Depolarization leads to dye release, resulting in decreased fluorescence. The mitochondrial membrane potential was assessed in pancreatic cells from the ALX-treated group that exhibited lower fluorescence spectra, indicating a decrease in mitochondrial membrane potential (MMP) (λ_{exi} = 510 nm; λ_{emi} = 525 nm) compared to the control group. NCHL pre-treatments outperformed CHL pre-treatments by preventing the decline in MMP, effectively restoring it to a nearly normal state in diabetic mice (Fig. 4a). To further confirm our investigations, the ATPase level in pancreatic tissue was determined from both the control and experimental groups. ALX exposure led to a significant decrease in ATP levels, indicated by higher ATPase levels in the ALX-treated group compared to controls. In contrast, ATPase levels were reduced in the CHL + ALX pre-treated groups, while NCHL pre-treatment effectively increased ATP levels in pancreatic tissue (Fig. 4b). Next, the calcium ion influx in the pancreatic tissues was investigated, which showed significant findings associated with mitochondrial functioning. The NCHL pre-treated groups (NCHL + ALX treatment) exhibited significantly higher intracellular calcium levels in pancreatic tissues compared to the ALX-treated group. NCHL effectively increased these calcium levels more than the CHL pre-treatment (Fig. 4c). Changes in Rh123 fluorescence intensity reliably quantify

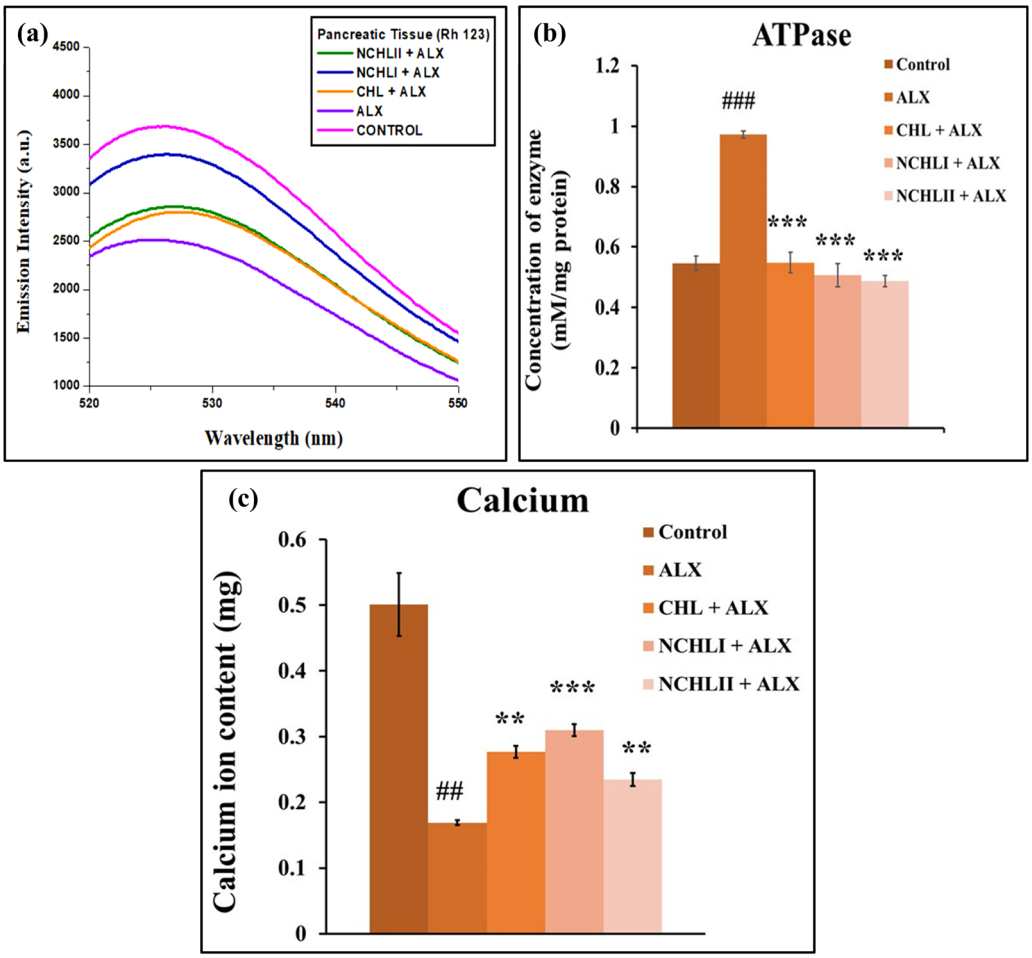

Fig. 4 Analysis of mitochondrial dysfunction: (a) quantification of mitochondrial membrane potential in pancreatic cells in control and different experimental mice groups by Rh 123 staining, (b) assessment of ATPase enzyme levels and the corresponding ATPase activity in control and experimental groups of mice. $^{###}p < 0.001$ *vs.* control; $^{***}p$ 0.001 *vs.* ALX; were considered significant for Student's *t*-test, and (c) analysis of intra-cellular calcium level in control and different experimental mice groups. $^{##}p < 0.01$ *vs.* control; $^{***}p < 0.001$, $^{**}p < 0.01$ *vs.* ALX, were considered significant for Student's *t*-test.

mitochondrial depolarization, making it a key marker for detecting mitochondrial dysfunction. Using this approach, findings confirmed that CHL protects against ALX-induced mitochondrial damage by stabilizing ATPase activity and maintaining calcium influx essential for insulin secretion. ALX disrupts insulin release by inhibiting glucokinase, impairing glycolysis, and altering ATP-sensitive K^+ (K^{ATP}) channels, thereby reducing calcium entry into pancreatic β-cells. Multiparametric studies showed that CHL effectively restored enzymatic profiles altered by ALX, while reduced ATPase activity in drug treated mice groups further emphasized NCHL's role in preserving mitochondrial function. These results collectively suggest that NCHL aids in maintaining glucose homeostasis and holds therapeutic promise for diabetes management.

Role of NCHL in targeting p53, Bcl2, Cyt *c*, and CYP1A1 signaling axis

According to other reports, ALX-induced diabetes propagates *via* oxidative DNA damage leading to genotoxicity and the associated apoptotic signaling mechanism. In addition to it, loss of mitochondrial membrane potential has been reported to be a biomarker of bioenergetic stress that results in the release of apoptotic factors leading to apoptotic cell death. ALX treatment led to increased Cyt *c* and CYP1A1 protein expression and decreased Bcl2 expression, which is an indicator of oxidative stress and apoptotic cell death. Here, the ALX that enters the pancreatic beta cell due to gluco-mimetic property, gets converted into a more toxic agent *i.e.* dilauric acid. This toxic derivative of ALX triggers hyper-activation of CYP1A1 protein

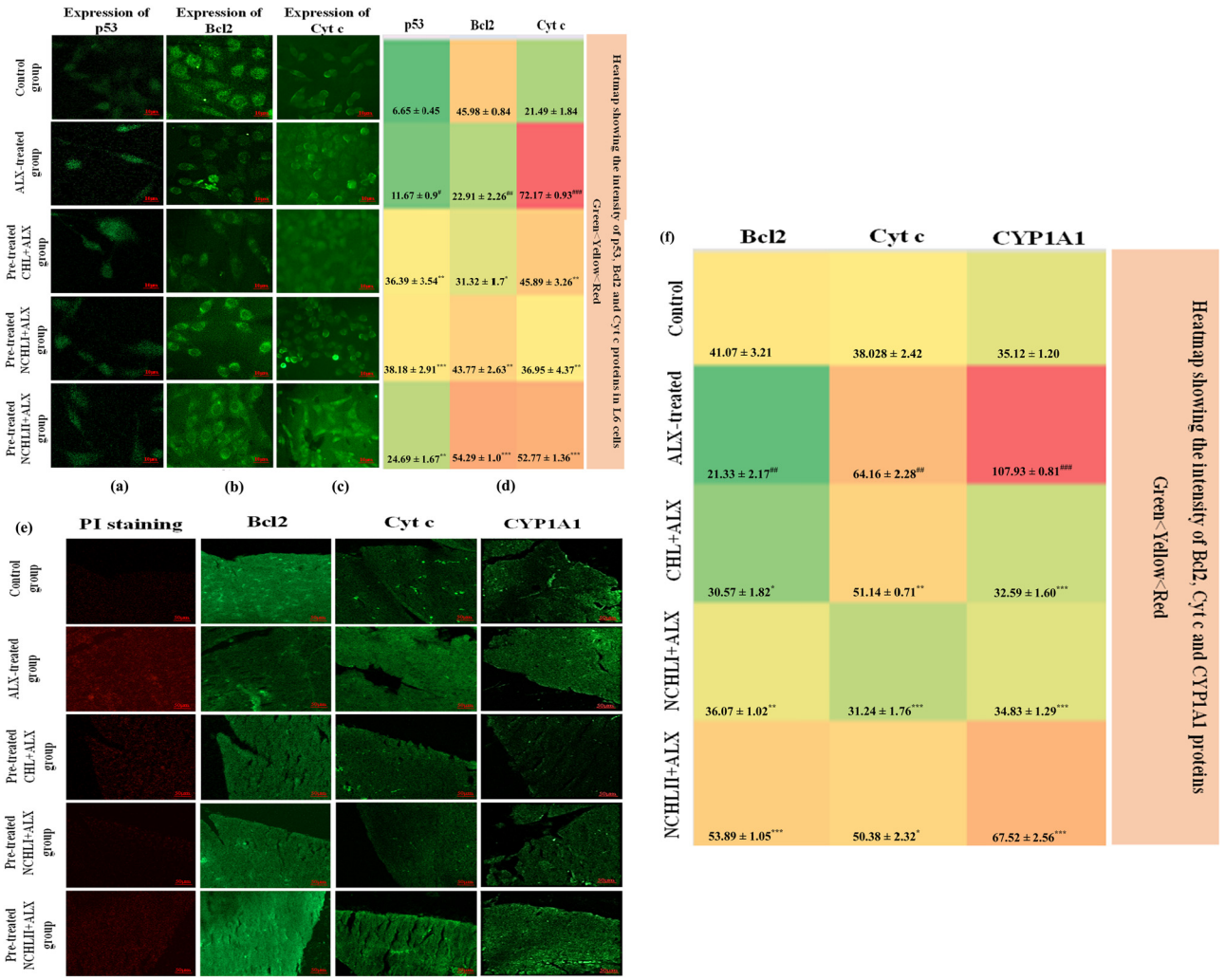

Fig. 5 Analysis of expression patterns of signaling proteins by the immunofluorescence study of: (a) p53 protein, (b) Bcl2 protein and (c) Cyt *c* protein expression level in L6 cells of control and different experimental sets, (d) image of heat-map showing the intensity of p53, Bcl2 and Cyt *c* protein expression levels in L6 cells of control and different experimental groups. Red colour represents a higher value, yellow colour represents a moderate value and green colour represents a lower value in the expression level of the proteins, (e) Bcl2, Cyt *c* and CYP1A1 protein expression levels in pancreatic tissue of control and different experimental groups of mice, (f) image of heat-map showing the intensity of Bcl2, Cyt *c* and CYP1A1 protein expression levels in pancreatic tissue of mice. Red colour represents a higher value, yellow colour represents a moderate value and green colour represents a lower value in the expression level of the proteins; $^{###}p < 0.001$, $##p < 0.01$, $^{#}p < 0.05$ *vs.* control, $***p < 0.001$, $**p < 0.01$, $*p < 0.05$ *vs.* ALX were considered significant for Student's *t*-test.

and leads to the generation of ROS after going through subsequent redox reactions and ultimately promotes oxidative stress in pancreatic mitochondria. This disrupts the normal functioning of mitochondria by modulating the expression and activity of Bcl2 and Cyt *c* protein, ultimately leading to pancreatic cell death (Fig. S1a, ESI†). The immunofluorescence studies using confocal microscopy revealed that L6 cells pre-treated with NCHLI and NCHLII exhibited higher p53 protein expression after ALX exposure compared to those treated with ALX alone (Fig. 5a). This suggests that NCHL pre-treatment may enhance p53 production, a key DNA damage response protein that protects against genotoxic stress, which corroborates with the ALX-induced genotoxicity studies. The NCHL groups also showed increased Bcl2 (Fig. 5b) and decreased Cyt *c* (Fig. 5c) expression compared to the ALX-only group, indicating better protection against ALX-induced mitochondrial dysfunction associated cell death. Statistical evaluations and significance analysis of the protein expression intensities represented as heat maps highlighted NCHL's potential in mitigating hyperglycemia linked to mitochondrial impairment in L6 cells (Fig. 5d). Additionally, an expression study of CYP1A1 protein was performed since it is regulated due to the presence of any environmental toxicant that promotes the formation of reactive oxygen species. The *in vivo* observations with immunofluorescence assay revealed heightened expression of Bcl2 and CYP1A1 proteins in both CHL and NCHL pre-treated groups, while Cyt *c* expression was reduced compared to ALX-treated mice. NCHL + ALX groups showed significantly lower fluorescence intensity, indicating improved protection against ALX-induced nuclear condensation and cell death through the synergistic effects of Bcl2 and Cyt *c*. CYP1A1, involved in metabolizing environmental toxins and ROS production, was elevated in ALX-induced mice but decreased in CHL and NCHL groups, suggesting the NCHL's superior protective role against mitochondrial ROS (Fig. 5e). Statistical evaluations of protein expression intensities from experimental mice were presented as heat maps, highlighting CHL's potential for modulating these signaling pathways to mitigate ALX-induced hyperglycemia (Fig. 5f). Therefore, the findings indicate that NCHL plays a crucial role in preventing genotoxic stress induced reactive oxygen species generation, mitochondrial dysfunction and abnormal programmed cell death in the pancreas, which corroborates with the cell viability (Fig. S1a and b, ESI†) and anti-oxidative enzymatic studies (Fig. S3, ESI†). The immunofluorescence analyses of different proteins underscore NCHL as a potential protective agent against diabetes-related complications by targeting the Bcl2/Cyt *c*/CYP1A1 signaling pathway.

Conclusions

This study investigates the health risks associated with synthetic food additives, particularly ALX which is known to induce diabetes by damaging pancreatic β cells through oxidative stress-induced mitochondrial dysfunction and genotoxicity. To counter these effects, this research explores the use of plant-based compound CHL as a cost-effective and non-toxic solution. Pre-treatment with these compounds delayed hyperglycemia and mitigated ALX-induced toxicity by optimizing enzymatic profiles, stabilizing mitochondrial function and modulating key proteins involved in DNA repair and apoptosis. Employing a biodegradable polymer, poly-lactide-*co*-glycolide (PLGA), for nano-encapsulation enhanced the bioavailability and efficacy of CHL allowing effective treatment even at reduced doses. However, the primary limitation of this study lies in the fact that the experimental findings need an ample amount of time to be extrapolated to higher animal model/clinical trials under real-world conditions as per ethical guidelines. Participant's behavior in controlled laboratory settings sometimes differs from those in natural environments, needing an extra time for trial and error, and dose standardization thereby delaying their applicability to broader clinical contexts. Nonetheless, the results of this work suggest that nano-formulated chlorophyllin (NCHL) offers promising therapeutic strategies for managing diabetes and its associated complications by targeting oxidative stress and mitochondrial dysfunction, paving the way for environmentally friendly, nature-based pharmacological interventions and would definitely benefit the pre-diabetics to delay their transformation to diabetic condition and also help the diabetics to foster a less complicated life, which flags on the urgency of active collaboration with clinical professionals to further advance the research through appropriately guided clinical trials.

Author contributions

All the authors contributed equally to this paper as follows: projection and conceptualization of the study: AS, PG, and SN; methodology and data curation: SD, RD, and PS, formal data analysis: SD, RD, PS, and AC; funding acquisition: AS; investigation: SD, RD, BB, and AC; methodology and project administration: SD; supervision of the *in vivo* study: AS; supervision of bio-physical studies: PG, and MB; bio-physical studies: MB and SS; resources: AS, PG, MB, and SN; software related to bio-physical studies: MB; software related to *in vivo* analysis: AS; visualization: SD, AS, PG, and SN; writing, reviewing, editing and final formatting of manuscript: SD, AS, PG, and MB; and overall supervision: AS, PG, and SN.

Data availability

The authors shall provide the data upon reasonable request.

Conflicts of interest

The authors have no conflicts of interest to disclose.

Acknowledgements

The authors would like to acknowledge SERB (DST), India (Grant No. ECR/2017/000355/LS) and UGC, New Delhi, India for the UGC-BSR (Grant No: F.30-488/2019(BSR)) sanctioned to

Dr Asmita Samadder for this research work. The authors are also thankful to the University of Kalyani, India for providing the Personal Research Grant (PRG) and DST-PURSE Contingency Grant, which were partly used for the research work. SD, PS, RD and SS extend their thankfulness to UGC for the SRF-fellowship. AC extends gratefulness to Kalyani University for the University Research Scholarship (URS). BB is grateful to the Govt. of West Bengal for the SVMCM fellowship. The authors also acknowledge the Department of Zoology, Department of Chemistry and S.N. Bose Innovation Centre (Central instrumentational facility) of the University of Kalyani for providing us with instrumentational support. The authors also extend their gratefulness towards UGC-DAE Consortium for Scientific Research, Kolkata Centre and Viswa-Bharati University for their infrastructural support and providing necessary research facilities.

References

1 M. A. Atkinson and G. S. Eisenbarth, Type 1 diabetes: new perspectives on disease pathogenesis and treatment, *Lancet*, 2001, **358**, 221–229.
2 S. V. Edelman, Type II diabetes mellitus, *Adv. Intern. Med.*, 1998, **43**, 449–500.
3 B. M. Popkin, L. S. Adair and S. W. Ng, Global nutrition transition and the pandemic of obesity in developing countries, *Nutr. Rev.*, 2012, **70**, 3–21.
4 P. Z. Zimmet, Diabetes and its drivers: the largest epidemic in human history?, *Clin. Diabetes Endocrinol.*, 2017, **3**, 1.
5 C. Rask-Madsen and G. L. King, Vascular complications of diabetes: mechanisms of injury and protective factors, *Cell Metab.*, 2013, **17**, 20–33.
6 T. C. Joseph and J. Vadasseril, Diabetes-A Silent Killer: A Threat for Cardiorespiratory Fitness, *Cardiorespiratory Fitness – New Topics*, IntechOpen, 2023.
7 R. Micha, S. K. Wallace and D. Mozaffarian, Red and Processed Meat Consumption and Risk of Incident Coronary Heart Disease, Stroke, and Diabetes Mellitus: A Systematic Review and Meta-Analysis, *Circulation*, 2010, **121**, 2271–2283.
8 S. Dey, A. Samadder and S. Nandi, Exploring Current Role of Nanotechnology Used in Food Processing Industry to Control Food Additives and their Biochemical Mechanisms, *Curr. Drug Targets*, 2022, **23**, 513–539.
9 S. E. Swithers, Artificial sweeteners produce the counterintuitive effect of inducing metabolic derangements, *Trends Endocrinol. Metab.*, 2013, **24**, 431–441.
10 R. Walker and J. R. Lupien, The Safety Evaluation of Monosodium Glutamate, *J. Nutr.*, 2000, **130**, 1049S–1052S.
11 K. He, S. Du, P. Xun, S. Sharma, H. Wang, F. Zhai and B. Popkin, Consumption of Monosodium Glutamate in Relation to Incidence of Overweight in Chinese Adults: China Health and Nutrition Survey (CHNS), *Am. J. Clin. Nutr.*, 2011, **93**, 1328–1336.
12 J. S. Dunn, J. Kirkpatrick, N. G. B. McLetchie and S. V. Telfer, Necrosis of the islets of Langerhans produced experimentally, *J Pathol. Bacteriol.*, 1943, **55**, 245–257.
13 V. Giaccone, G. Cammilleri, V. Di Stefano, R. Pitonzo, A. Vella, A. Pulvirenti, G. M. Lo Dico, V. Ferrantelli and M. Macaluso, First report on the presence of Alloxan in bleached flour by LC-MS/MS method, *J. Cereal Sci.*, 2017, **77**, 120–125.
14 K. Wadkar, C. Magdum, S. Patil and N. Naikwade, Antidiabetic potential and Indian medicinal plants, *J. Herb. Med. Toxicol.*, 2008, **2**, 45–50.
15 B. Salehi, A. Ata, N. V. Anil Kumar, F. Sharopov, K. Ramírez-Alarcón, A. Ruiz-Ortega, S. Abdulmajid Ayatollahi, P. V. Tsouh Fokou, F. Kobarfard, Z. Amiruddin Zakaria, M. Iriti, Y. Taheri, M. Martorell, A. Sureda, W. N. Setzer, A. Durazzo, M. Lucarini, A. Santini, R. Capasso, E. A. Ostrander, A. ur-Rahman, M. I. Choudhary, W. C. Cho and J. Sharifi-Rad, Antidiabetic Potential of Medicinal Plants and Their Active Components, *Biomolecules*, 2019, **9**, 551.
16 A. Rodriguez-Casado, The Health Potential of Fruits and Vegetables, Phytochemicals: Notable Examples, *Crit. Rev. Food Sci. Nutr.*, 2014, **56**, 1097–1107.
17 J. Das, A. Samadder, J. Mondal, S. K. Abraham and A. R. Khuda-Bukhsh, Nano-encapsulated chlorophyllin significantly delays progression of lung cancer both in in vitro and in vivo models through activation of mitochondrial signaling cascades and drug-DNA interaction, *Environ. Toxicol. Pharmacol.*, 2016, **46**, 147–157.
18 A. Patra and M. Bera, Spectroscopic investigation of new water soluble Mn^{II}_2 and Mg^{II}_2 complexes for the substrate binding models of xylose/glucose isomerases, *Carbohydr. Res.*, 2014, **384**, 87–98.
19 S. Haldar, A. Patra and M. Bera, Exploring the catalytic activity of new water soluble dinuclear copper(II) complexes towards the glycoside hydrolysis, *RSC Adv.*, 2014, **4**, 62851–62861.
20 W. Fan, B. Yung, P. Huang and X. Chen, Nanotechnology for multimodal synergistic cancer therapy, *Chem. Rev.*, 2017, **117**, 13566–13638.
21 S. Lukasiewicz, K. Szczepanowicz, K. Podgorna, E. Blasiak, N. Majeed, S. O. O. Ogren, W. Nowak, P. Warszynski and M. Dziedzicka-Wasylewska, Encapsulation of clozapine in polymeric nanocapsules and its biological effects, *Colloids Surf., B*, 2016, **140**, 342–352.
22 M. Teixeira, M. J. Alonso, M. M. M. Pinto and C. M. Barbosa, Development and characterization of PLGA nanospheres and nanocapsules containing xanthone and 3-methoxyxanthone, *Eur. J. Pharm. Biopharm.*, 2005, **59**, 491–500.
23 S. A. Saadia, H. A. Khan, A. S. Ghazanfar and K. Saadatullah, Alloxan induced diabetes in rabbits, *Pak. J. Pharmacol.*, 2005, **22**, 41–45.
24 O. M. Ighodaro, A. M. Adeosun and O. A. Akinloye, Alloxan-induced diabetes, a common model for evaluating the glycemic-control potential of therapeutic compounds and plants extracts in experimental studies, *Medicina*, 2017, **53**, 365–374.

25 A. Samadder, S. K. Abraham and A. R. Khuda-Bukhsh, Nanopharmaceutical approach using pelargonidin towards enhancement of efficacy for prevention of alloxan-induced DNA damage in L6 cells via activation of PARP and p53, *Environ. Toxicol. Pharmacol.*, 2016, **43**, 27–37.

26 J. Das, A. Samadder, S. Das, A. Paul and A. R. Khuda-Bukhsh, Nanopharmaceutical approach for enhanced anticancer activity of betulinic acid in lung-cancer treatment via activation of PARP: interaction with dna as a target: -anticancer potential of nano-betulinic acid in lung cancer, *J. Pharmacopunct.*, 2016, **19**, 37–44.

27 H. Fessi, F. Puisieux, J. P. Devissaquet, N. Ammoury and S. Benita, Nanocapsule formation by interfacial polymer deposition following solvent displacement, *Int. J. Pharm.*, 1989, **55**, 1–4.

28 A. Samadder, S. Das, J. Das and A. R. Khuda-Bukhsh, Relative efficacies of insulin and poly (lactic-*co*-glycolic) acid encapsulated nano-insulin in modulating certain significant biomarkers in arsenic intoxicated L6 cells, *Colloids Surf., B*, 2013, **109**, 10–19.

29 A. Samadder, B. Bhattacharjee, S. Dey, A. Chakrovorty, R. Dey, P. Sow, D. Tarafdar, M. Biswas and S. Nandi, Enhanced Drug Carriage Efficiency of Curcumin-Loaded PLGA Nanoparticles in Combating Diabetic Nephropathy via Mitigation of Renal Apoptosis, *J. Pharmacopunct.*, 2024, **27**, 1–13.

30 C. A. Lamey, N. Moussa, M. W. Helmy, M. Haroun and S. A. Sabra, Simultaneous encapsulation of dasatinib and celecoxib into caseinate micelles towards improved in vivo anti-breast cancer efficacy with reduced drug toxicity, *J. Drug Delivery Sci. Technol.*, 2023, **87**, 04807.

31 J. Das, S. Das, A. Samadder, K. Bhadra and A. R. Khuda-Bukhsh, Poly (lactide-*co*-glycolide) encapsulated extract of Phytolacca decandra demonstrates better intervention against induced lung adenocarcinoma in mice and on A549 cells, *Eur. J. Pharm. Sci.*, 2012, **47**, 313–324.

32 A. Mukherjee and B. Singh, Binding interaction of pharmaceutical drug captopril with calf thymus DNA: a multispectroscopic and molecular docking study, *J. Lumin.*, 2017, **190**, 319–327.

33 M. Khorasani-Motlagh, M. Noroozifar and S. Khmmarnia, Study on fluorescence and DNA-binding of praseodymium (III) complex containing 2,2′-bipyridine, *Spectrochim. Acta, Part A*, 2011, **78**, 389–395.

34 A. M. Nowicka, E. Zabost, M. Donten, Z. Mazerska and Z. Stojek, Electroanalytical and spectroscopic procedures for examination of interactions between double stranded DNA and intercalating drugs, *Anal. Bioanal. Chem.*, 2007, **389**, 1931–1940.

35 D. Sarkar, P. Das, S. Basak and N. Chattopadhyay, Binding interaction of cationic phenazinium dyes with calf thymus DNA: A comparative study, *J. Phys. Chem.*, 2008, **112**, 9243–9249.

36 L. A. Kaplan, Carbohydrates and metabolite, in *Clinical Chemistry: Theory, Analysis And Co-Relation*, L. A. Kaplan, A. J. Pesce, S. C. Kazmierczak, Mosby, St. Louis, 1984, 4th edn, pp. 1032–1040.

37 A. Samadder, D. Chakraborty, A. De, S. S. Bhattacharyya, K. Bhadra and A. R. Khuda-Bukhsh, Possible signalling cascades involved in attenuation of alloxan-induced oxidative stress and hyperglycemia in mice by ethanolic extract of Syzygium jambolanum: Drug-DNA interaction with calf thymus DNA as target, *Eur. J. Pharm. Sci.*, 2011, **44**, 207–217.

38 J. Solomon, R. J. Bulkley and J. Mayer, Effect of a low dose of alloxan on blood glucose, islet beta cell granulation, body weight, and insulin resistance of ob/ob mice, *Diabetologia*, 1974, **6**, 709–715.

39 H. S. Parmar and A. Kar, Antidiabetic potential of Citrus sinensis and Punica granatum peel extracts in alloxan treated male mice, *BioFactors*, 2007, **1**, 17–24.

40 A. Samadder, S. Dey, P. Sow, R. Das, S. Nandi, J. Das, B. Bhattacharjee, A. Chakrovorty, M. Biswas and P. Guptaroy, Phyto-chlorophyllin Prevents Food Additive Induced Genotoxicity and Mitochondrial Dysfunction via Cytochrome *c* Mediated Pathway in Mice Model, *Comb. Chem. High Throughput Screening*, 2021, **2**, 1618–1627.

41 S. Dey, P. Sow, R. Dey, P. Guptaroy, S. Nandi and A. Samadder, Design, synthesis and therapeutic exploration of nanocurcumin targeting the synergistic interactions with p53 and PARP-1 proteins in preventing food-additive induced genotoxicity and diabetic complications, *Colloids Surf., A*, 2025, 136230.

42 J. Zheng, J. He, B. Ji, Y. Li and X. Zhang, Antihyperglycemic activity of Prunella vulgaris L. in streptozotocin-induced diabetic mice, *Asia Pac. J. Clin. Nutr.*, 2007, **16**, 427–431.

43 S. S. Bhattacharyya, S. Paul and A. R. Khuda-Bukhsh, Encapsulated plant extract (Gelsemium sempervirens) PLGA nanoparticles enhance cellular uptake and increase bioactivity *in vitro*, *Exp. Biol. Med.*, 2010, **235**, 678–688.

44 A. Berraaouan, Z. Abderrahim, M. Hassane, L. Abdelkhaleq, A. Mohammed and B. Mohamed, Evaluation of Protective Effect of Cactus Pear Seed Oil (Opuntia Ficus-Indica L. MILL.) Against Alloxan-Induced Diabetes in Mice, *Asian Pac. J. Trop. Med.*, 2015, **8**, 532–537.

45 A. Kaplan and L. S. Lavernel, Lipid metabolism, in *Clinical Chemistry: Interpretations and techniques*, Lea and Febiger, Philadelphia, 1983, 2nd edn, pp. 333–336.

46 H. U. Bergmeyer and E. Brent, *Methods in enzymatic analysis*, Academic Press, 1974, vol. 2, p. 735.

47 S. Das, J. Das, A. Samadder, A. Paul and A. R. Khuda-Bukhsh, Strategic formulation of apigenin-loaded PLGA nanoparticles for intracellular trafficking, DNA targeting and improved therapeutic effects in skin melanoma in vitro, *Toxicol. Lett.*, 2013, **223**, 124–138.

48 A. Dhawan, N. Mathur and P. K. Seth, The effect of smoking and eating inhibit on DNA damage in Indian populations as measured in the comet assay, *Mutat. Res.*, 2001, **474**, 121–128.

49 A. R. Khuda-Bukhsh, S. S. Bhattacharyya, S. Paul, S. Dutta, N. Boujedaini and P. Belon, Modulations of signal proteins: A plausible mechanism to explain how a potentized drug Secale Cor 30C diluted beyond Avogadro's limit combats skin papilloma in mice, *J. Evidence-Based Complementary Altern. Med.*, 2009, **2011**, 41.

50 P. Banerjee, S. J. Biswas, P. Belon and A. R. Khuda-Bukhsh, A Potentized Homeopathic Drug, Arsenicum Album 200, Can Ameliorate Genotoxicity Induced by Repeated Injections of Arsenic Trioxide in Mice, *J. Vet. Med. Sci.*, 2007, **54**, 370–376.

51 H. Ohakawa, N. Ohishi and K. Yagi, Assay for lipid peroxides in animal tissues by thiobarbituric acid reaction, *Anal. Biochem.*, 1979, **95**, 351–358.

52 P. Kakkar, B. Das and P. N. Viswanathan, A modified spectrophotometric assay of superoxide dismutase, *Indian J. Biochem. Biophys.*, 1984, **21**, 130–132.

53 A. C. Maehly and B. Chance, The assay of catalase and peroxidase, *Methods Biochem. Anal.*, 1954, **1**, 357–424.

54 A. Samadder, D. Tarafdar, R. Das, A. R. Khuda-Bukhsh and S. K. Abraham, Efficacy of nanoencapsulated pelargonidin in ameliorating pesticide toxicity in fish and L6 cells: modulation of oxidative stress and signalling cascade, *Sci. Total Environ.*, 2019, **671**, 466–473.

55 A. Majumder, N. Dutta, S. Dey, P. Sow, A. Samadder, G. Vijaykumar, K. Rangan and M. Bera, A Family of [Zn6] Complexes from the Carboxylate-Bridge-Supported Assembly of [Zn2] Building Units: Synthetic, Structural, Spectroscopic, and Systematic Biological Studies, *Inorg. Chem.*, 2021, **60**, 17608–17626.

56 S. Dey, I. Nagpal, P. Sow, R. Dey, A. Chakrovorty, B. Bhattacharjee, S. Saha, A. Majumder, M. Bera, N. Subbarao, S. Nandi, S. Hossen Molla, P. Guptaroy, S. K. Abraham, A. R. Khuda-Bukhsh and A. Samadder, Morroniside interaction with poly (ADP-ribose) polymerase accentuates metabolic mitigation of alloxan-induced genotoxicity and hyperglycaemia: a molecular docking based in vitro and in vivo experimental therapeutic insight, *J. Biomol. Struct. Dyn.*, 2024, **42**, 8541–8558.

57 R. R. Ishmukhametov, J. B. Pond, A. Al-Huqail, M. A. Galkin and S. B. Vik, ATP synthesis without R210 of subunit a in the Escherichia coli ATP synthase, *Biochem. Biophys. Acta*, 2008, **1777**, 32–38.